

Thermal neutron cross sections of amino acids from average contributions of functional groups

Giovanni Romanelli,¹ Dalila Onorati,^{2, a)} Pierfrancesco Ulpiani,³ Stephanie Cancelli,⁴ Enrico Perelli-Cippo,⁴ José Ignacio Márquez Damián,⁵ Silvia C. Capelli,¹ Gabriele Croci,^{4, 6} Andrea Muraro,⁶ Marco Tardocchi,⁶ Giuseppe Gorini,⁴ Carla Andreani,^{2, 7} and Roberto Senesi^{2, 8}

¹⁾ISIS Neutron and Muon Source, UKRI-STFC, Rutherford Appleton Laboratory, Harwell Campus, Didcot, Oxfordshire OX11 0QX, United Kingdom

²⁾Università degli Studi di Roma “Tor Vergata”, Dipartimento di Fisica and NAST Centre, Via della Ricerca Scientifica 1, Roma 00133, Italy

³⁾Università degli Studi di Roma “Tor Vergata”, Dipartimento di Scienze e Tecnologie Chimiche, Via della Ricerca Scientifica 1, Roma 00133, Italy

⁴⁾Università di Milano-Bicocca, Piazza della Scienza 3, Milano, Italy

⁵⁾European Spallation Source ERIC, P.O. Box 176, 22100 Lund, Sweden

⁶⁾Istituto per la Scienza e Tecnologia dei Plasmi, CNR, via Cozzi 53, 20125 Milano, Italy

⁷⁾CNR-ISM, Area della Ricerca di Roma Tor Vergata, Via del Fosso del Cavaliere 100, 00133 Roma, Italy

⁸⁾CNR-IPCF, Sezione di Messina, Viale Ferdinando Stagno d’Alcontres 37, Messina, 98158, Italy

(Dated: 12 February 2021)

The experimental thermal neutron cross sections of the twenty proteinogenic amino acids have been measured over the incident-neutron energy range spanning from 1 meV to 10 keV and data have been interpreted using the multi-phonon expansion based on first-principles calculations. The scattering cross section, dominated by the incoherent inelastic contribution from the hydrogen atoms, can be rationalised in terms of the average contributions of different functional groups, thus neglecting their correlation. These results can be used for modelling the total neutron cross sections of complex organic systems like proteins, muscles, or human tissues from a limited number of starting input functions. This simplification is of crucial importance for fine-tuning of transport simulations used in medical applications, including boron neutron capture therapy as well as secondary neutrons-emission induced during proton therapy. Moreover, the parametrized neutron cross sections allow a better treatment of neutron scattering experiments, providing detailed sample self-attenuation corrections for a variety of biological and soft-matter systems.

I. INTRODUCTION

The study of the interaction of neutrons with matter has still to become centennial, yet it has impacted the modern society in a variety of ways, from fission reactors to the creation of isotopes for medical care; from the treatment of cancer to the non-invasive characterization of cultural-heritage artworks; as well as the scientific investigation of the structure and dynamics of condensed-matter systems^{1, 2}. In the latter case, special attention should be paid to hydrogen (¹H) for it manifests the largest bound scattering cross section (82.03 barn) amongst the elements of the periodic table³. For this reason, neutron scattering off hydrogen is particularly relevant, for example, for molecular spectroscopy⁴ and catalysis⁵, hydrogen storage⁶, and cultural heritage⁷.

Fermi was the first to model the interaction potential between slow neutrons (energies lower than few eV) and hydrogenous solids⁸. He explicitly discussed how the total cross sections, $\sigma(E)$, for neutrons with incident energy E , would change by approximately a factor of 4 when moving from cold neutrons to epithermal ones. On the one hand, epithermal neutrons (eV – keV) have energies much larger than the typical

binding energy of hydrogen in a crystal or molecular system, therefore resulting in a Compton-like scattering from an approximately free nucleus^{9–14}. In this case, the scattering is defined as elastic in the neutron + nucleus system, thus requiring the conservation of kinetic energy and momentum of both particles, and the total scattering cross section corresponds to the free-nucleus value, σ_f . On the other hand, cold neutrons ($\mu\text{eV} - \text{meV}$) impinging on a cold solid sample would bounce off an almost unmovable target. Therefore, as such neutrons do not change their kinetic energy following the interaction, the scattering is elastic in the system composed solely by the neutron, and the total scattering cross section corresponds to the bound-nucleus value, $\sigma_b = \sigma_f(1 + m/M)^2$, where m is the mass of the neutron, and M the mass of the nucleus. This corresponds, in the case of hydrogen, to $\sigma_b \simeq 4\sigma_f$.

In the intermediate (thermal) energy region, the scattering is elastic in neither of the two cases aforementioned, for part of the neutron kinetic energy can be transferred to rotational or internal vibrations of a molecule, or lattice and to phonon modes in a crystal, in a regime generally referred to as inelastic neutron scattering⁴. For crystalline samples, the cross section also depends on the structure via the presence of Bragg edges. Moreover, while the picture drawn by Fermi holds exactly for solids at low temperatures, the total scattering cross section at energies lower than tens of meV can be higher than σ_b in a solid at room or higher temperature, following the

^{a)}Corresponding Author: dalila.onorati@uniroma2.it

population of the Stokes and anti-Stokes transitions related to the vibrational modes, according to the Maxwell-Boltzmann statistics. In a liquid, furthermore, contributions from diffusion motions can increase additionally $\sigma(E)$ at values of E below some meV.

Tabulated Thermal Cross Sections (TCS) are available for just a handful of systems^{15–17}. In order to match the level of detail in modern Monte Carlo nuclear transport codes, the possibility to calculate TCS from simplified models¹⁸, from molecular dynamics¹⁹, as well as from *ab initio* calculations^{20–26} has been a topic of recent development. Despite the important effort redirected into the theoretical calculation of TCS, the experimental data available for comparison and validation of the models is quite scarce. Moreover, new experimental investigations, aimed to update decades-old data, are clearly needed, as recently demonstrated for the case of parahydrogen²⁷. In this context, a sustained experimental programme has been started at the VESUVIO spectrometer^{28–30} at the ISIS Neutron and Muon Source (UK)³¹, to investigate TCS of alcohols³², organic systems³³, water^{34,35} and other materials used to moderate neutrons^{36–39}. The unprecedentedly broad energy range for incident neutrons available at the instrument²⁸, spanning from a fraction of meV to tens of keV, allows a complete characterization of total neutron cross sections, from cold to epithermal neutrons. Moreover, the broad energy range provides an accurate and self-consistent way to normalize the experimental spectra for those samples whose density is more difficult to determine²⁹, such as powders or samples experiencing *in situ* adsorption⁴⁰ or phase transitions.

In this framework, the measurement and calculation of TCS of a vast set of materials are challenging tasks, owing to the several non-trivial dependencies on the molecular structure, dynamics, and thermodynamic temperature. When the TCS calculation is applied to human tissues or muscles for applications such as Boron Neutron Capture Therapy (BNCT)^{41,42} as well as to study secondary neutrons-emission induced during proton therapy^{43,44}, the possibility to reconstruct the cross section of large proteins becomes challenging. In fact, the 20 basic amino acids can combine to form tens of thousands⁴⁵ up to several billions of proteins⁴⁶, making the task of either calculate or measure the entire set of related TCS unrealistic.

Here we provide an experimental determination of the total TCS of the twenty amino acids, as a function of the neutron energy from a fraction of meV to tens of keV, together with first-principles calculations based on the incoherent approximation, thus particularly suitable for hydrogen-containing materials. Given such unprecedentedly consistent set of experimental data, we attempt a rationalization of the TCS of amino acids and, by extension, of proteins, as a set of average contributions of independent functional groups, such as CH_n , NH_n , and OH . The process of average over the amino acids allows to consider the functional groups as independent, and to obtain the final results directly by adding the different contributions from different functional groups, neglecting their correlations. We will refer to this procedure as the Average Functional Group Approximation, AFGA. This task would allow the replication of complex TCS, *e.g.*, for biophysical and medical applications, having just a handful of initial param-

ters.

II. MATERIALS AND METHODS

A. Neutron experiment

Neutron-transmission experiments were performed at the VESUVIO spectrometer at the ISIS Neutron and Muon Source. All the 20 amino acids were commercially available in their L-form from Sigma Aldrich⁴⁷ as anhydrous powders. Samples were loaded as received in circular flat containers with Nb faces perpendicular to the direction of the neutron beam, and Al spacers defining the sample volume. The latter corresponded to a cylindrical shape with thickness of either 1 or 2 mm for all samples, and a circular area facing the beam with diameter 5 cm, thus covering the entire circular beam profile²⁸. All samples were measured at the temperature of 300 K within the instrument’s closed-circuit refrigerator. For each sample, data were collected for about 0.5–1.5 hours, corresponding to an integrated proton current of 90–270 μAh within the ISIS synchrotron. The values of mass, thickness and integrated proton current are reported in Table I, together with the molecular stoichiometry. Time-of-flight spectra of incident neutrons not interacting with the sample were obtained using the standard GS20 ⁶Li-doped scintillator available at the instrument, as well as the newly installed double thick Gas Electron Multiplier (GEM) detector⁴⁸. The latter was positioned between the sample position and the GS20 monitor, at a distance from the moderator of 12.60 m, as calibrated at the beginning of the experiment using the VESUVIO incident foil changer²⁹. The GS20 transmission monitor and the sample positions correspond to 13.45 m and 11.00 m, respectively²⁸. It is important to stress that, for most of the samples investigated in the present experiment, transmission spectra from both the GS20 monitor and the GEM detector were available at the same time, and provided concurrent measurements of the neutron cross section of the same sample using two independent equipments. Given the distances of both detectors, the counts due to multiple scattering events within the sample are completely negligible as compared to experimental errors bars²⁹.

Moreover, the GEM detector allowed more precise measurements over the extended energy range available at the instrument, down to 0.6 meV, corresponding to the so-called empty neutron pulse at the Target Station 1 at ISIS²⁸, as compared to 3 meV of the GS20 detector. This is a consequence of the lower sensitivity to γ -rays in the GEM compared to scintillators like the traditional GS20 monitor.

Transmission spectra were obtained, as a function of the incident neutron energy, using the Beer-Lambert law, as

$$T(E) = \alpha \frac{S(E)}{C(E)} = \exp(-n\sigma(E)d), \quad (1)$$

where $S(E)$ and $C(E)$ are the spectra corresponding to sample inside the container and empty container, respectively. Moreover, n is the number density of molecules inside the sample

Amino Acid	Formula	CH ₃	CH ₂	CH	Zw. ⁺	Other	σ_f [barn]	%H	M [g]	d [mm]	Q [μ Ah]	Structure
Leucine	C ₆ H ₁₃ NO ₂	2	1	2	NH ₃	–	312.08	85.3	1.63	1.00	270	Ref. ⁴⁹
Isoleucine	C ₆ H ₁₃ NO ₂	2	1	2	NH ₃	–	312.08	85.3	3.89	2.00	180	Ref. ⁵⁰
Valine	C ₅ H ₁₁ NO ₂	2	–	2	NH ₃	–	266.40	84.6	3.41	1.00	270	Ref. ⁵¹
Methionine	C ₅ H ₁₁ NO ₂ S	1	2	1	NH ₃	S	267.36	84.3	2.97	2.00	90	Ref. ⁵²
Lysine	C ₆ H ₁₄ N ₂ O ₂	–	4	1	NH ₃	NH ₂	342.58	83.7	3.60	1.00	270	Ref. ⁵³
Threonine	C ₄ H ₉ NO ₃	1	–	2	NH ₃	OH	224.46	82.1	5.02	2.00	90	Ref. ⁵⁴
Alanine	C ₃ H ₇ NO ₂	1	–	1	NH ₃	–	175.03	81.9	4.35	2.00	1080	Ref. ⁵⁵
Cysteine	C ₃ H ₇ NO ₂ S	–	1	1	NH ₃	SH	176.00	81.5	5.30	2.00	180	Ref. ⁵⁶
Serine	C ₃ H ₇ NO ₃	–	1	1	NH ₃	OH	178.78	80.2	6.02	2.00	90	Ref. ⁵⁷
Proline	C ₅ H ₉ NO ₂	–	3	1	NH ₂	–	225.44	80.1	2.25	1.00	180	Ref. ⁵⁸
Glycine	C ₂ H ₅ NO ₂	–	1	–	NH ₃	–	129.35	79.2	4.54	2.00	270	Ref. ⁵⁹
Arginine	C ₆ H ₁₄ N ₄ O ₂	–	3	1	NH ₂	(NH ₂) ₂ , NH	362.63	79.1	3.46	1.00	270	Ref. ⁶⁰
Glutamic Acid	C ₅ H ₉ NO ₄	–	2	1	NH ₃	OH	232.93	79.1	4.16	2.00	270	Ref. ⁶¹
Phenylalanine	C ₉ H ₁₁ NO ₂	–	1	6	NH ₃		285.30	79.0	6.28	2.00	90	Ref. ⁶²
Glutamine	C ₅ H ₁₀ N ₂ O ₃	–	2	1	NH ₃	NH ₂	259.68	78.9	2.89	2.00	450	Ref. ⁶³
Tyrosine	C ₉ H ₁₁ NO ₃	–	1	5	NH ₃	OH	289.00	77.9	2.12	2.00	180	Ref. ⁶⁴
Aspartic Acid	C ₄ H ₇ NO ₄	–	1	1	NH ₃	OH	187.23	76.6	5.05	2.00	270	Ref. ⁶⁵
Asparagine	C ₄ H ₈ N ₂ O ₃	–	1	1	NH ₃	NH ₂	214.00	76.6	5.39	2.00	180	Ref. ⁶⁶
Tryptophan	C ₁₁ H ₁₂ N ₂ O ₂	–	1	6	NH ₃	NH	325.23	75.6	3.05	2.00	270	Ref. ⁶⁷
Histidine	C ₆ H ₉ N ₃ O ₂	–	1	3	NH ₃	NH	250.20	72.7	4.69	2.00	270	Ref. ⁶⁸

TABLE I. Chemical formula and decomposition of L-amino acids, together with the total value of the free scattering cross section per formula unit, σ_f , as well as the relative amount of hydrogen atoms per formula unit. The amino acids are generally found in their Zwitterion form, the cation is reported in the column labelled Zw.⁺, and the formula unit is completed by adding the anion, COO^- . For each sample are reported the values of mass (± 0.01 g) and thickness (± 0.05 mm) together with the integrated proton current. The reference providing the crystal structure used in the *ab initio* simulations is also reported in the last column.

volume, $\sigma(E)$ is their energy-dependent total cross section, and d the thickness of the container. Finally, α is a normalization factor taking into account the different durations of the measurements with and without the sample. In the case of the GS20 monitor, α is an energy-dependent normalization provided by the measurement of the incident neutron beam by the instrument monitor at 8.57 m from the moderator, before the sample position. In the case of the GEM detector, both $S(E)$ and $C(E)$ were normalized to the number of proton pulses counted by the detector electronics. However, as a slight fluctuation of the efficiency with time is known to affect the GEM detector⁴⁸, of magnitude ca. 2% with no dependence upon the neutron energy, the resulting transmission spectra were scaled so as to overlap to the GS20 spectra for epithermal neutrons.

B. Calculations of thermal cross sections

Within the incoherent approximation^{69–71}, the double differential scattering cross section can be expressed as a sum of single-particle contributions weighted by the sum of coherent and incoherent bound scattering cross sections³ for each isotope j , $\sigma_{b,j}$, namely

$$\frac{d^2\sigma}{d\mu dE'} = \sqrt{\frac{E'}{E}} \sum_j N_j \frac{\sigma_{b,j}}{2} S_j(\vec{Q}, \omega), \quad (2)$$

where μ is the cosine of the scattering angle, E and E' are the initial and final neutron energies, N_j represents the stoichiometry

of the sample, and $S_j(\vec{Q}, \omega)$ is known as scattering law (or scattering kernel) as function of the energy, $\hbar\omega = E - E'$ and momentum, \vec{Q} , transfers. This approximation is particularly suitable for hydrogen-rich materials, as in the present case, for the incoherent scattering contribution from hydrogen sums up to ca. 99% of the total. Moreover, we adopt the powder-average approximation for non-oriented samples, thus we will consider the scattering law as a function of the modulus of the momentum transfer, Q , but not of its direction.

$S_j(Q, \omega)$ is made explicit by defining the Fourier transform of the intermediate self-scattering function. Sjolander showed that, in a harmonic cubic Bravais lattice and within the Gaussian approximation, the scattering law can be expressed as^{69,70}

$$S_j(Q, \omega) = e^{-2W_j} \sum_{n=0}^{\infty} \frac{(2W_j)^n}{n!} H_n(\omega), \quad (3)$$

where $H_0(\omega) = \delta(\omega)$,²²

$$H_1(\omega) = \frac{g_j(\omega)}{\hbar\omega \gamma_j(0)} \frac{1}{2} \left[\coth\left(\frac{\hbar\omega}{2k_B T}\right) + 1 \right] \quad (4)$$

and

$$H_{n>1}(\omega) = \int H_1(\omega') H_{n-1}(\omega - \omega') d\omega'. \quad (5)$$

This procedure describes the so-called Multi-Phonon Expansion (MPE), where the n -th term represents the contribution from the scattering process involving n phonons. Thus, the

first term gives the elastic cross-section; the next term gives the cross-section for all one-phonon processes in which, in turn, each phonon is excited; and so on. The function $g_j(\omega)$ represents the unit-area normalized Vibrational Density of States (VDoS) of a given nucleus, such that $g_j(\omega)d\omega$ is the fraction of the normal modes whose frequencies lie in the range between ω and $\omega + d\omega$. Moreover, in Eq. 3,

$$\gamma_j(0) = \int_0^\infty \frac{g_j(\omega)}{\hbar\omega} \coth\left(\frac{\hbar\omega}{2k_B T}\right) d\omega, \quad (6)$$

is also used to define the so-called Debye-Waller factor, $2W_j$,⁷² with the relation

$$2W_j = \langle (\vec{Q} \cdot \vec{u}_j) \rangle = \frac{1}{3} Q^2 \langle u_j^2 \rangle = E_{R,j} \gamma_j(0), \quad (7)$$

where $E_{R,j} = \hbar^2 Q^2 / 2M_j$, $\langle u_j^2 \rangle$ is the mean square displacement, and the second equality holding within the isotropic approximation.

In principle, the MPE can be calculated up to any value of n , yet its numerical evaluation becomes progressively more time-consuming. In fact, as the incident energy increases, an increasingly large number of phonons is likely to be involved in the scattering process. However, in the epithermal region the neutron scattering cross section can be interpreted in the Impulse Approximation (IA)⁷³ and the scattering law can be expressed as

$$S_{IA,j}(Q, \omega) = \frac{\exp\left(-\frac{(\hbar\omega - E_{R,j})^2}{4E_{R,j}k_B T_j}\right)}{\sqrt{4\pi E_{R,j}k_B T_j}}, \quad (8)$$

where $E_{R,j}$ is interpreted, within the IA, as the nucleus recoil energy, and T_j is an effective temperature proportional to the kinetic energy of the scattering nucleus. In this work, we have adopted the transition energy between the MPE and the IA equal to 3 eV. In particular, above this energy and only for the evaluation of the total scattering cross section, the value of T_j can be approximated with T , the same thermodynamic temperature used in the MPE. Otherwise, at lower values of E , substantially higher values of T_j should be used³² in the case of hydrogen well above room temperature (see *e.g.*, Ref.⁷⁴⁻⁷⁷) and for heavier masses up to room temperature (see *e.g.*, Refs.⁷⁸⁻⁸¹)

The total scattering cross-section $\sigma(E)$ is obtained by combining Eqs. 3 and 8 with Eq. 2, integrating over the values of μ , in the range $[-1, 1]$, and over E' . The VDoS can be obtained from first-principles computer simulations, as discussed in the next section. From a numerical point of view, it is important to note that the limit of energy integration is only formally extended to infinity because the integrand differs from zero only in a finite interval up to the cut-off energy $\hbar\omega_C = n\hbar\omega_m$, with $\hbar\omega_m$ the highest vibrational frequency in the VDoS. Furthermore, each term $H_n(\omega)$ is unit-area normalized. Finally, the total cross section is obtained by adding the neutron absorption cross section. By neglecting any nuclear resonance, not expected for H, C, O, S and N in the range investigated in this experiment, the absorption contribution has a simple form $\sigma_{a,j}(E) = \sigma_{a,j} \sqrt{E_0/E}$, where the

values of $\sigma_{a,j}$, corresponding to the absorption at $E_0 = 25.3$ meV, can be adopted from Ref.³. Therefore,

$$\sigma(E) = \int d\mu \int dE' \frac{d^2\sigma}{d\mu dE'} + \sum_j N_j \sigma_{a,j}(E). \quad (9)$$

C. Phonon calculations

The VDoS used in the MPE to estimate the TCS was obtained from *ab initio* simulations using the Quantum Espresso (QE)⁸² code, with a $6 \times 6 \times 6$ k-grid in the first Brillouin zone of the crystal structure. The pseudopotentials used were taken from Ref.⁸³, while the crystal structures for each amino acids were taken from the Refs. reported in Table I.

A Density Functional Perturbation Theory (DFPT) calculation was run on the optimized geometry, the output corresponded to a collection of eigenvalues of the molecular normal modes, ω_ν , and eigenvectors representing each atomic motion for a given normal mode, $\vec{e}_{\nu,j}$. The index ν spans between 1 and $3N - 3$ normal modes, where N is the number of atoms in the unit cell and where we neglected the three lowest-energy translational modes. The atom-projected VDoS for atom j is obtained as

$$g_j(\omega) = \sum_\nu \delta(\omega - \omega_\nu) e_{\nu,j}^2, \quad (10)$$

where $e_{\nu,j}^2$ is the square modulus of the eigenvector of j -nucleus corresponding to the ν -vibration. In particular, the quantities $\vec{e}_{\nu,j} = \sqrt{M_j} \vec{u}_{\nu,j}$ are obtained from the dynamical matrix and are associated to the eigenvalue frequency ω_ν . Finally, $\vec{u}_{\nu,j}$ is the related atomic displacement, expressed as the difference of the time-dependent and mean nuclear positions. Additional details regarding the calculation of eigenvectors and eigenfrequencies were reported in Ref.^{84,85}.

One should note that the *ab initio* simulations provide substantial additional information with respect to the experiment, as one can analyse the VDoS for each nucleus in the molecule separately. Such functions can either be averaged over nuclei of the same element, such as H, N, C, S and O in the present case, or they can be averaged for nuclei in the same functional group and over different molecules, such as H in a CH₃ methyl group.

III. RESULTS

The experimental neutron transmission spectra of all amino acids were interpreted according to Eq. 1. In particular, the value of $-\ln(T(E > 3 \text{ eV}))$ was normalised to the constant free scattering cross section of the molecule,

$$\sigma_f = \sum_j N_j \sigma_{f,j}, \quad (11)$$

where $\sigma_{f,j}$ is the free scattering cross section for isotope j , and N_j the related stoichiometry. This is a fundamental tool

available at the VESUVIO spectrometer, for it allows a self-consistent normalization of the data not based on the measured sample density, dependent on the powder grain size and packing fraction, and quite different from the tabulated one for the bulk crystal. The values of the bound cross sections for H, O, C, N, and S were taken from³, and we considered for each element the values averaged over the naturally abundant isotopes.

Figure 1 shows the experimental total cross sections of (from top to bottom) glutamic acid (A) and aspartic acid (B); cysteine (C) and glycine (D); and valine (E) and alanine (F). For each sample, the results obtained using the GS20 and GEM monitors agree, within error bars, over the neutron energy range spanning from 3 meV to 10 eV. For the investigated energies higher than 10 eV, up to 10 keV, all cross sections are found to be constant, as expected. Importantly, the new GEM detector allows a more precise determination of $\sigma(E)$ in two key regions. First, more accurate data are obtained at energies between 0.6 meV and 3 meV, using the empty-pulse at ISIS Target Station 1²⁸ where the spectra collected by the GS20 can be affected by an important environmental gamma background^{86–88}, especially for samples with high scattering power. Yet, owing to the lower sensitivity to γ -rays provided by the GEM detector, the data collected with this new addition are of exquisite quality. The second region where the new detector provides a relevant improvement to the VESUVIO instrument corresponds to epithermal neutrons. Here, the higher efficiency of the detector allows a higher count rate, thus smaller experimental error bars and less scattering of the data points around the value of the free scattering cross section. This is of particular importance for experiments involving powder samples, as in this case, for it improves the normalization procedure based on Eq. 11 and discussed in Ref.²⁹.

The experimental data in Figure 1 were compared to the predictions from the MPE and IA, as discussed earlier. In particular, two models were tested for the scattering contributions: model 1 (m1) applies the MPE to all elements in the molecule; while model 2 (m2) combines the result from the MPE applied to hydrogen only and the values of the free scattering cross sections, $\sigma_{f,i}$ for the elements i other than hydrogen. As one can appreciate from the comparison in Figure 1, both models compare extremely well to the experimental data, and they differ only slightly one from the other. In particular, the values from model 1 are found to be, for all amino acids, slightly larger than those from model 2, as expected, and also slightly larger than the experimental data. One should note that the MPE applied to the elements heavier than hydrogen is more sensitive to the lower-energy part of $g_i(\omega)$, where the atom-projected VDoS is more intense. Following the $1/\omega$ dependence in Eq. 6, one can expect that a slight error in the calculation of the intensities of $g_i(\omega \rightarrow 0)$ becomes particularly evident on the final result, and especially at higher values of T . It is also important to note that the calculation of $\sigma(E)$ using model 2, *i.e.*, applying the MPE only to hydrogen and using $\sigma_{f,i}$ for the other elements, provides a significantly simpler approach and substantially lower computational costs, yet obtaining a very accurate result. Experimental results for the neutron cross section of amino acids were previously pre-

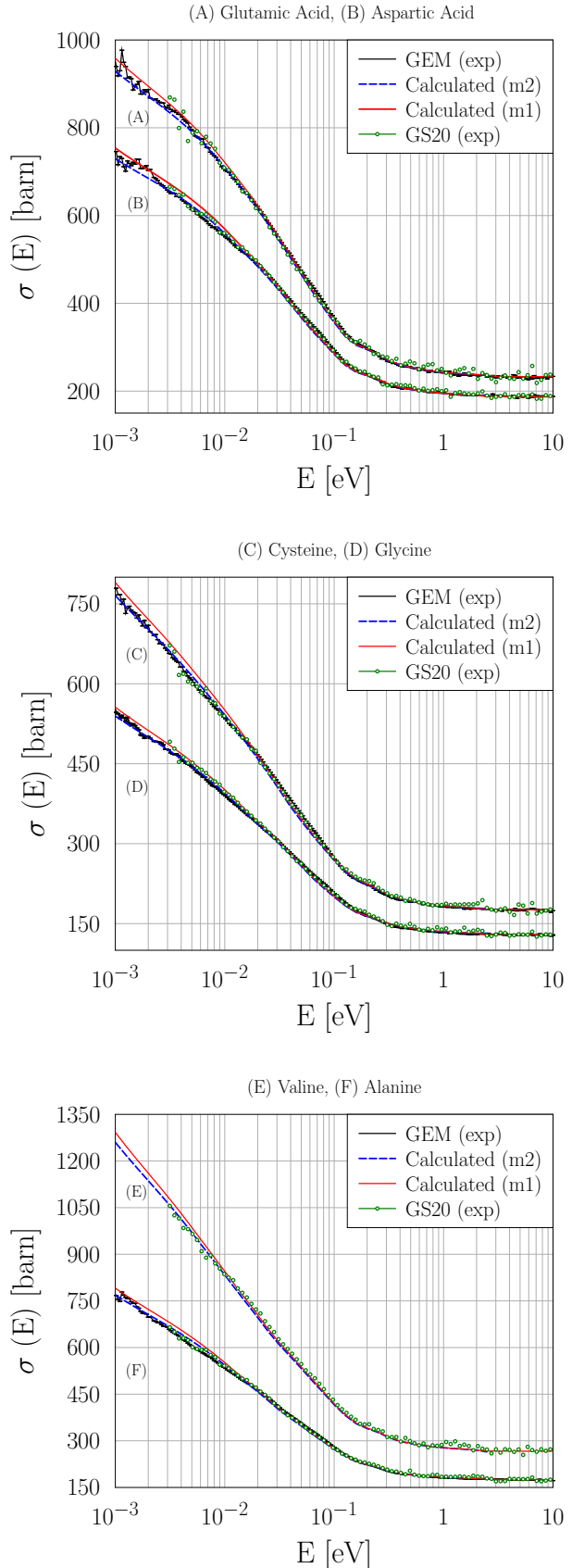


FIG. 1. The total cross section of glutamic acid (A) and aspartic acid (B); cysteine (C) and glycine (D); and valine (E) and alanine (F). For each sample, the experimental data from the GEM (black error bars) and GS20 monitors (green circles) are compared to the calculated spectra using model 1 (red continuous line) and model 2 (blue dashed line).

sented in Ref.⁸⁹ at one value of the incident neutron energy of 50 meV. We note that those results generally underestimate the results from the present investigation, possibly because of the uncertainties on the density and thickness of the powder samples avoided in our normalization procedure²⁹.

Finally, we note that all calculated cross sections were obtained by a newly created Python algorithm, based on the formalism explained in Section 2, and prepared in such a way that it can be readily included in the MantidPlot^{75,90} environment for the reduction and analysis of neutron experiments. In particular, the application of the script developed here would be suitable for the reduction and normalization algorithm presented in Ref.⁹¹. While the agreement between our calculations and the experimental results is a powerful benchmark of our algorithm, we performed additional comparisons applying the LEAPR module of NJOY2016¹⁷ to our VDoS. The results from our algorithm satisfactorily overlap with those obtained using NJOY2016, with a maximum difference in the case of glycine at 1 meV of about 0.7%, and, therefore are not shown here.

IV. DISCUSSION

A. Average Functional Group Approximation

A final, fundamental, comment regarding Figure 1 is related to the different features and energy dependence of the cross section of each amino acid. As mentioned earlier, this is the result of the different VDoSs that make, in principle, the determination of the cross section of proteins a challenging task. In particular, pioneering studies using inelastic neutron scattering already showed how the VDoS (thus the double-differential cross section, Eq. 2) of isolated amino acids could differ significantly from those of the related dipeptides⁹². However, when integrating Eq. 2 so as to obtain the total cross section, some sharp features and differences vanish. In this framework, we have interrogated our *ab initio* simulations so as to extract the contribution to the total cross section from hydrogen atoms in different functional groups within the molecule.

Figures 2 and 3 show the total cross section of hydrogen in different average functional groups, namely CH_n , NH_n , OH , and SH . In particular, the molecular structure of each amino acid simulated was interpreted according to the separation in functional groups reported in Table I. The total cross section from hydrogen atoms in the same or different amino acids but belonging to the same type of functional group were averaged, and for each value of the incident neutron energy, a standard deviation associated to this average was defined and corresponds to the error bars in the figures. The fact that signals from the functional groups are found to differ beyond the calculated error bars is an *a posteriori* proof that the averaging procedure was meaningful. One can appreciate, for example looking at the top panel of Figure 2, how the average contribution to the total cross section in a methylidyne ($\equiv\text{CH}$), methylene ($=\text{CH}_2$), and methyl groups ($-\text{CH}_3$) are markedly different one from the other. In particular, within the CH grouping,

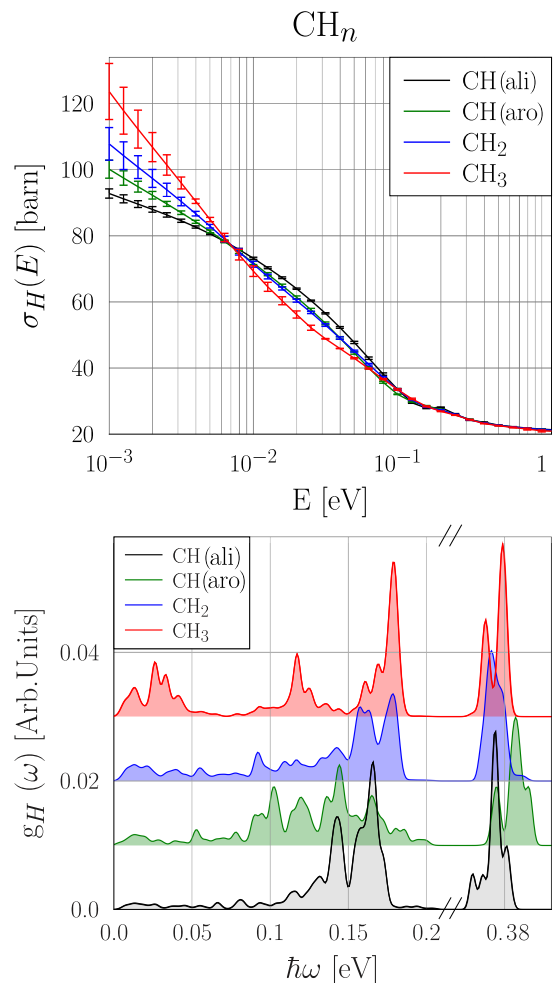


FIG. 2. Total cross section (top) and atom-projected VDoS (bottom) of hydrogen in CH_n functional groups, averaged over all amino acids presenting such groups. The VDoSs spectra are shifted in the y-scale for the sake of clarity.

one can distinguish the contributions from aliphatic CH and aromatic CH functional groups. This has to do with the different VDoSs in the four groups, as shown in Figure 2 (bottom). For example, the Stokes and anti-Stokes low-energy excitation and de-excitations corresponding to the CH_3 rotor in the methyl group are more easily populated at room temperature, and provide a higher value of the total cross sections at thermal-to-cold neutron energies. On the other hand, as all VDoSs are normalized to one, the larger cross section of hydrogen in a CH_3 group at neutron energies lower than ca. 7 meV has, as a counterpart, a depletion in the region between ca. 7 meV and ca. 90 meV. The opposite is true for the hydrogen in a methylidyne group, while hydrogen in a methylene group has intermediate values between the two previous cases. It is important to note that the average of cross sections over hydrogen atoms participating in same functional group is not identical, in principle, to the cross section obtained from the average of VDoSs of the same hydrogen atoms. However we have checked that the results obtained following these two

approaches, in the case of CH, CH₂ and CH₃, are the same within our numerical accuracy. For this reason, we report in the Supplementary Material the average VDoS of the functional groups considered so as to allow the calculation of the total cross sections at temperatures other than 300 K.

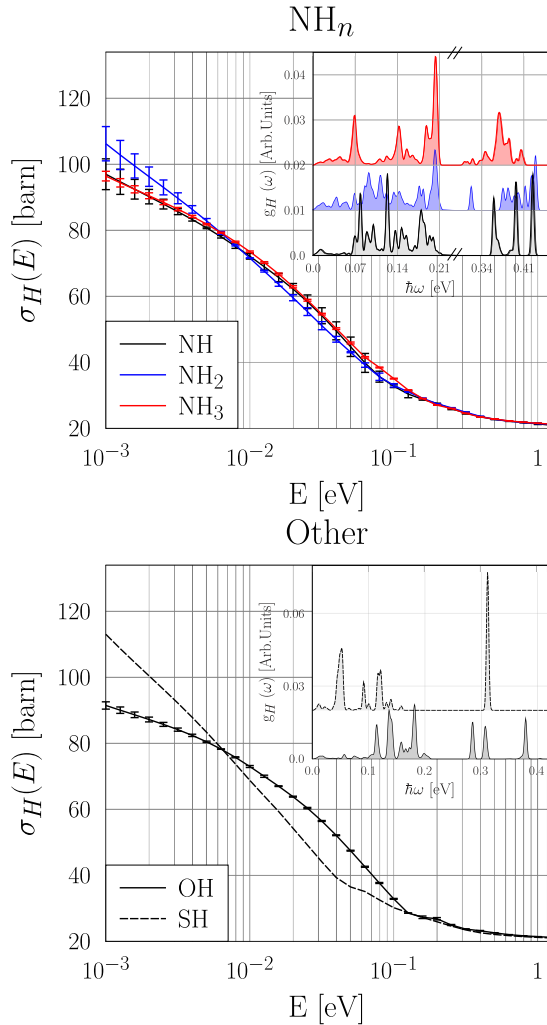


FIG. 3. Total cross section of hydrogen in NH_n, OH, and SH functional groups, averaged over all amino acids presenting such groups. In the inserts the respectively atom-projected VDoS.

The possibility to express the total cross section of amino acids as average contributions of independent functional groups allows, in principle, the possibility to accurately approximate the cross section of a given protein by the *a priori* knowledge of its composition and the set of 9 functions reproduced in Figures 2 and 3 and reported in the Supplementary Material from 1 meV to 1 eV. In order to test this approximation, we have compared the experimental cross sections of the 13 remaining amino acids with the predictions based on the AFGA. The results, presented in Figure 4, are also compared with the calculations using model 2. In general, the predictions compare extremely favourably to both experimental data and *ab initio* calculations based on model 2. Some differences arise for neutron energies lower than few meV, where

we find, in the case of lysine, a maximum difference of ca. 5% at 1 meV between the prediction based on the AFGA and the calculation based on model 2. As we have proved correct the AFGA for a large set of amino acids, one can expect that the same approximation will hold as well for larger proteins.

B. Application to other organic materials

Triphenylmethane (C₆H₅)₃CH is a material of great potential interest as neutron moderator. This molecular compound is composed by three phenyl groups connected through a central carbon atom. In the top panel of Figure 5, it is shown the comparison between the experimental hydrogen cross section of triphenylmethane, measured on VESUVIO from Ref.³⁷, and the predicted spectrum using the average cross section from aromatic CH functional group defined in our AFGA model. In the figure it is also reported the calculation, from Ref.³⁷, from NJOY2016 Nuclear Data Processing system using as input the VDoS obtained by DFT simulations. We note that the agreement of our results compared to experimental data and simulation is excellent, providing a successful test of AFGA also for molecular systems different from amino acids.

The bottom panel of Figure 5 shows the comparison between the neutron scattering cross section of polymethylmethacrylate, or lucite (C₅O₂H₈)_n, from Ref.⁹³ and the prediction based on the AFGA. To construct the total cross section based on the AFGA, we considered lucite as composed by non-interacting chains of CH₂C(CH₃)CO₂CH₃ units. The related DFT calculations from Ref.⁹³ were performed using CASTEP⁹⁴ and the output files were processed with OCLIMAX²⁵ to calculate the scattering law, then with NJOY2016¹⁷ to calculate the neutron scattering cross section using a procedure tested in other articles, *e.g.*, Ref.⁹⁵. In Figure 5 (bottom), the experimental data measured by Sibona *et al.*⁹⁶ are also reported, as well as the cross section tabulated in the ENDF/BVIII.0⁹⁷ library. A very good agreement between the experimental data and the reconstruction using our AFGA model has been found over the entire energy range, with a slight departure from the experimental data at neutron energies below few meV. In particular, the AFGA seems to provide a much better agreement than the results based on direct DFT simulations⁹³ in the broad region below ca. 100 meV. To explain this result, one should consider that lucite is, in reality, a non-crystalline vitreous substance and, therefore, its simulation using DFT-based phonon calculations can be quite challenging, unless very large unit cells are considered. On the other hand, the AFGA provides the scattering contribution of a given functional group averaged over a series of slightly different environments and, therefore, is more able to reproduce the disordered nature of the material at the atomic scale.

The successful application of the AFGA to materials not related to amino acids of proteins is of particular interest for possible applications to a broader family of systems, including glassy materials, and prove its general applicability. In fact, while it is not expected for the AFGA to provide a high level of accuracy for small crystalline systems, the averaging of

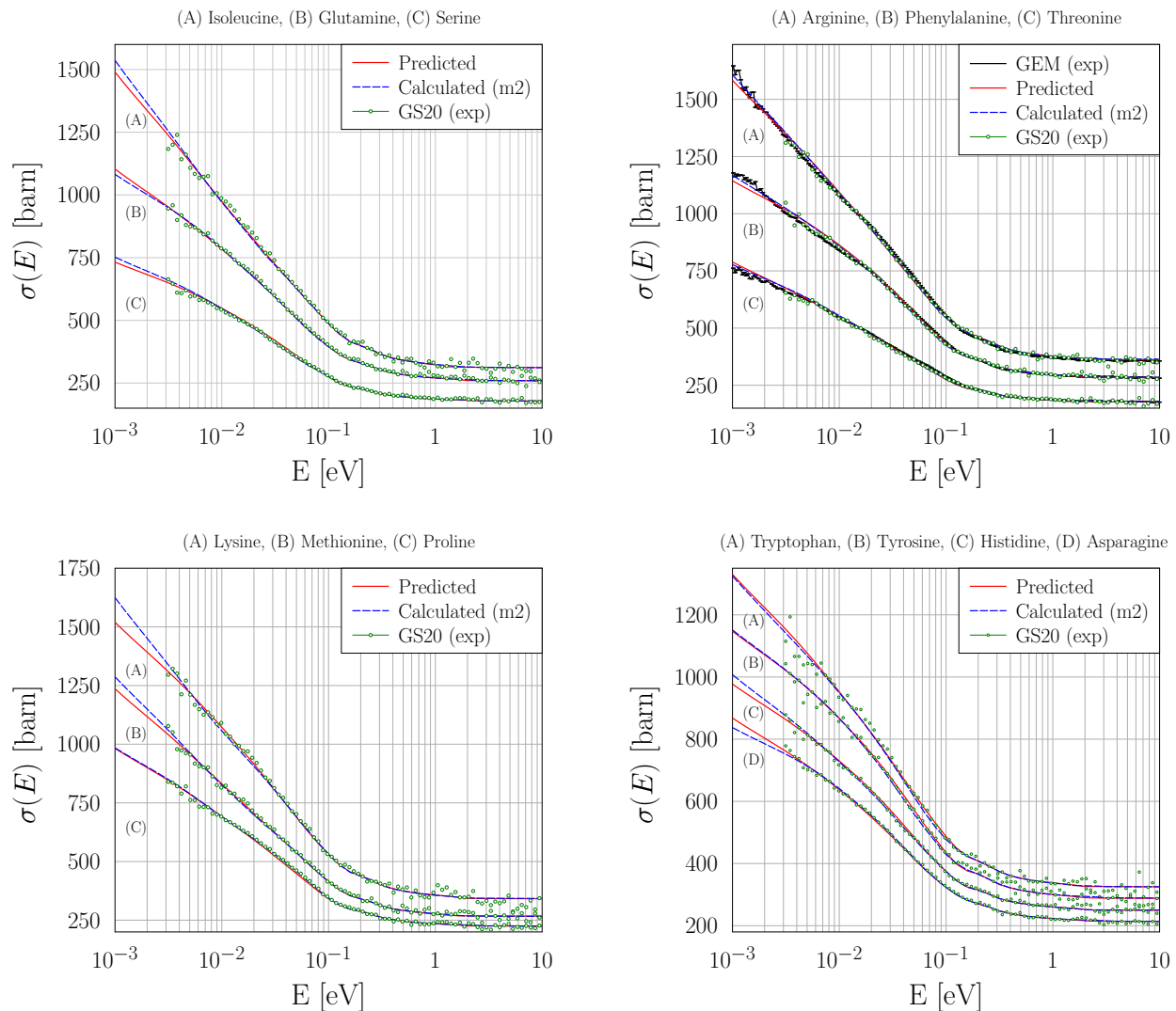


FIG. 4. Total neutron cross section for the 13 amino acids not reported in Figure 1. The results obtained using the Average Functional Group Approximation (AFGA, red line) are compared to the experimental results obtained using the GS20 (green circles) and GEM detector (black error bars). The results obtained applying model 2 (m2) to the specific phonon calculation of each molecule are also reported as blue dotted line.

contributions of individual functional groups in a set of “training” systems can be representative of both large molecule, polymers and disordered biophysical systems.

C. Modelling using a sigmoidal function

The definition of an average total cross section for hydrogen in organic systems, over the same energy range investigated here, was recently provided in Ref.³³. In that case, the hydrogen total cross section was averaged over several organic molecules, including β -alanine, urea, and tartaric acid, so as to take into account the average contributions over different functional groups. In order to provide a simple analytical model, the result was fitted with a logistic 4-parameter sig-

moidal function of the form

$$\sigma(E) \cong s_f + \frac{s_b}{1 + cE^d} \quad (12)$$

Considering the additional insight that we have gathered in this study, provided by the results of our *ab initio* calculations and the possibility to separate the signal from different functional groups, we have applied the same analytic function to each of 9 spectra obtained within the AFGA. The parameters obtained for all types of functional groups are shown in the Table II. They allow a better treatment of neutron scattering experiments, providing detailed sample self-attenuation corrections for a variety of biological and soft-matter systems.

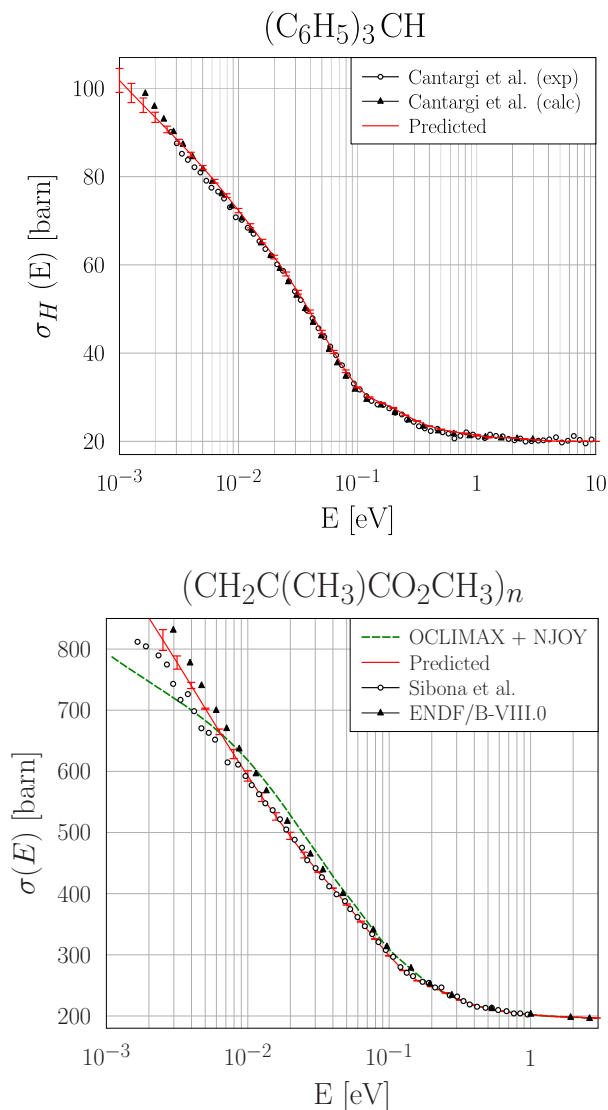


FIG. 5. Hydrogen neutron cross section in solid triphenyl-methane (top) from Ref.³⁷ and the prediction based on the AFGA. Total neutron scattering cross section of poly-methylmethacrylate or lucite (bottom) from Ref.⁹³ and the prediction based on the AFGA.

	s_f	s_b	c	d
CH(ali)	19.14 ± 0.6	73.11 ± 1	37.46 ± 6	1.03 ± 0.04
CH(aro)	17.51 ± 0.7	86.72 ± 2	28.62 ± 4	0.84 ± 0.04
CH ₂	16.20 ± 0.9	105.1 ± 3	23.40 ± 2	0.71 ± 0.03
CH ₃	13.60 ± 0.6	174.8 ± 7	27.14 ± 1	0.55 ± 0.02
NH ₃	18.82 ± 0.5	74.92 ± 1	32.90 ± 3	0.94 ± 0.03
NH ₂	17.54 ± 0.5	101.5 ± 2	28.75 ± 2	0.75 ± 0.02
NH	19.10 ± 0.6	78.09 ± 1	36.39 ± 4	0.95 ± 0.03
OH	19.27 ± 0.6	71.29 ± 1	44.57 ± 7	1.09 ± 0.05
SH	19.24 ± 0.4	107.3 ± 2	60.64 ± 5	0.85 ± 0.02

TABLE II. Fitted curve parameters of different hydrogen contributions to the cross-section averaged over all amino acids using a sigmoidal function.

V. CONCLUSIONS

We have provided experimental results for the total neutron cross section of the twenty proteinogenic amino acids in the neutron energy range between 1 meV and 10 keV. These were successfully reproduced applying the formalism of the multi-phonon expansion to the calculated vibrational densities of states obtained from *ab initio* simulations. Moreover, from the results of such calculations, we have defined the average contribution to the total cross section from hydrogen atoms in different functional groups. The set of 9 functions, defined by the average hydrogen dynamics in different chemical environments, was found to accurately reproduce the total cross section of all amino acids, in the framework named Average Functional Group Approximation, *i.e.*, AFGA. Moreover, we found that the AFGA could be successfully applied to triphenylmethane and poly-methylmethacrylate, or lucite, a glassy material for which phonon calculations are known to have limited success.

Our results represent a considerable simplification in the challenging task of reproducing the total neutron cross section of dipeptides and proteins, with applications to biophysics and medicine. For example, our results can be utilised to provide new models for the macroscopic cross section of human tissues and muscles, and for applications to the cancer treatment through boron neutron capture therapy.

VI. SUPPLEMENTARY MATERIAL

See the supplementary material for the values of the average hydrogen total cross section at 300 K and average VDoSs for functional groups in the AFGA model.

VII. DATA AVAILABILITY

Raw data related to this article were generated at the ISIS Neutron and Muon Source (UK), DOI: 10.5286/ISIS.E.RB2010019. Derived data supporting the findings of this study are available from the corresponding author upon reasonable request.

ACKNOWLEDGMENTS

The authors gratefully acknowledge the financial support of Regione Lazio (IR approved by Giunta Regionale n. G10795, 7 August 2019 published by BURL n. 69 27 August 2019), ISIS@MACH (I), and ISIS Neutron and Muon Source (UK) of Science and Technology Facilities Council (STFC); the financial support of Consiglio Nazionale delle Ricerche within CNR-STFC Agreement 2014-2020 (N 3420), concerning collaboration in scientific research at the ISIS Neutron and Muon Source (UK) of Science and Technology Facilities Council (STFC) is gratefully acknowledged.

The following article has been submitted to Journal of Chemical Physics. After it is published, it will be found at <https://aip.scitation.org/journal/jcp>.

REFERENCES

- ¹C. Andreani, J. C. Dore, and F. P. Ricci, “Structural characterization of diatomic fluids by diffraction studies,” *Rep. Prog. Phys.* **54**, 731 (1991).
- ²F. Fernandez-Alonso and D. L. Price, *Neutron Scattering – Fundamentals* (Academic Press, New York, 2013).
- ³V. F. Sears, “Neutron scattering lengths and cross sections,” *Neutron News* **3**, 26–37 (1992).
- ⁴P. C. H. Mitchell, *Vibrational spectroscopy with neutrons: with applications in chemistry, biology, materials science and catalysis*, Vol. 3 (World Scientific, 2005).
- ⁵I. P. Silverwood, S. F. Parker, and C. R. A. Catlow, “Neutron scattering in catalysis and energy materials,” *Phys. Chem. Chem. Phys.* **18**, 17140–17140 (2016).
- ⁶A. Ramirez-Cuesta, M. Jones, and W. David, “Neutron scattering and hydrogen storage,” *Mater. Today* **12**, 54–61 (2009).
- ⁷G. Festa, G. Romanelli, R. Senesi, L. Arcidiacono, C. Scatigno, S. F. Parker, M. P. M. Marques, and C. Andreani, “Neutrons for cultural heritage—techniques, sensors, and detection,” *Sensors* **20** (2020).
- ⁸E. Fermi, “La ricerca scientifica,” *Riv. del Nuovo Cim.* **13**, 434–439 (1936).
- ⁹J. M. F. Gunn, C. Andreani, and J. Mayers, “A new approach to impulsive neutron scattering,” *J. Phys. C* **19**, L835 (1986).
- ¹⁰S. Imberti, C. Andreani, V. Garbuio, G. Gorini, A. Pietropaolo, R. Senesi, and M. Tardocchi, “Resolution of the VESUVIO spectrometer for High-energy Inelastic Neutron Scattering experiments,” *Nucl. Instrum. Methods Phys. Res. A* **522**, 463 (2005).
- ¹¹M. A. Ricci, M. Nardone, A. Fontana, C. Andreani, and W. Hahn, “Light and neutron scattering studies of the OH stretching band in liquid and supercritical water,” *J. Chem. Phys.* **108**, 450–454 (1998).
- ¹²C. Andreani, D. Colognesi, J. Mayers, G. F. Reiter, and R. Senesi, “Measurement of momentum distribution of light atoms and molecules in condensed matter systems using inelastic neutron scattering,” *Adv. Phys.* **54**, 377–469 (2005).
- ¹³C. Andreani, M. Krzystyniak, G. Romanelli, R. Senesi, and F. Fernandez-Alonso, “Electron-volt neutron spectroscopy: beyond fundamental systems,” *Adv. Phys.* **66**, 1–73 (2017).
- ¹⁴C. Andreani, R. Senesi, M. Krzystyniak, G. Romanelli, and F. Fernandez-Alonso, “Chapter 7 - atomic quantum dynamics in materials research,” in *Neutron Scattering - Applications in Biology, Chemistry, and Materials Science*, Experimental Methods in the Physical Sciences, Vol. 49, edited by F. Fernandez-Alonso and D. L. Price (Academic Press, 2017) pp. 403–457.
- ¹⁵J. Koppel, J. Triplett, and Y. Naliboff, “Gasket: A unified code for thermal neutron scattering,” General Dynamics Corp., San Diego, Calif. General Atomic Div. (1967).
- ¹⁶R. E. Macfarlane, “New thermal neutron scattering files for endf/b-vi release 2,” Los Alamos National Laboratory report LA-12639-MS (ENDF-356) (1994).
- ¹⁷R. Macfarlane, D. W. Muir, R. M. Boicourt, A. C. Kahler, III, and J. L. Conlin, “The njoy nuclear data processing system, version 2016,” Los Alamos National Laboratory report LA-UR-17-20093 (2017).
- ¹⁸J. R. Granada, “Slow-neutron scattering by molecular gases: A synthetic scattering function,” *Phys. Rev. B* **31**, 4167–4177 (1985).
- ¹⁹J. M. Damian, D. C. Malaspina, and J. R. Granada, “Vibrational spectra of light and heavy water with application to neutron cross section calculations,” *J. Chem. Phys.* **139**, 024504 (2013).
- ²⁰A. Hawari, I. Al-Qasir, V. Gillette, B. Wehring, and T. Zhou, “Ab initio generation of thermal neutron scattering cross sections,” *Proc. PHYSOR 2004*, 25–29 (2004).
- ²¹A. Hawari, “Modern techniques for inelastic thermal neutron scattering analysis,” *Nuclear Data Sheets* **118**, 172–175 (2014).
- ²²X.-X. Cai and E. Klinkby, “Neutron total cross section calculation within the framework of quasi-harmonic approximation,” *New J. Phys.* **19**, 103027 (2017).
- ²³Wormald, Jonathan and Hawari, Ayman I., “Thermal neutron scattering law calculations using ab initio molecular dynamics,” *EPJ Web Conf.* **146**, 13002 (2017).
- ²⁴I. Al-Qasir, V. Gillette, and A. Qteish, “Thermal neutron scattering kernels for uranium mono-nitride: A potential advanced tolerant fuel candidate for light water reactors,” *Ann. Nucl. Energy* **127**, 68–78 (2019).
- ²⁵Y. Q. Cheng, L. L. Daemen, A. I. Kolesnikov, and A. J. Ramirez-Cuesta, “Simulation of inelastic neutron scattering spectra using oclimax,” *J. Chem. Theory Comput.* **15**, 1974–1982 (2019).
- ²⁶Y. Q. Cheng and A. J. Ramirez-Cuesta, “Calculation of the thermal neutron scattering cross-section of solids using oclimax,” *J. Chem. Theory Comput.* **16**, 5212–5217 (2020).
- ²⁷K. Grammer, R. Alarcon, L. Barrón-Palos, D. Blyth, J. Bowman, J. Calarco, C. Crawford, K. Craycraft, D. Evans, N. Fomin, *et al.*, “Measurement of the scattering cross section of slow neutrons on liquid parahydrogen from neutron transmission,” *Phys. Rev. B* **91**, 180301 (2015).
- ²⁸G. Romanelli, M. Krzystyniak, R. Senesi, D. Raspino, J. Boxall, D. Pooley, S. Moorby, E. Schooneveld, N. J. Rhodes, C. Andreani, and F. Fernandez-Alonso, “Characterisation of the incident beam and current diffraction capabilities on the vesuvio spectrometer,” *Meas. Sci. Technol.* **28**, 095501 (2017).
- ²⁹J. Robledo, J. Dawidowski, J. M. Damián, G. Škoro, C. Bovo, and G. Romanelli, “Measurement of neutron total cross sections at the vesuvio spectrometer,” *Nucl. Instrum. Methods Phys. Res., Sect. A* **969**, 164096 (2020).
- ³⁰P. Ulpiani, G. Romanelli, D. Onorati, A. Parmentier, G. Festa, E. Schooneveld, C. Cazzaniga, L. Arcidiacono, C. Andreani, and R. Senesi, “Optimization of detection strategies for epithermal neutron spectroscopy using photon-sensitive detectors,” *Rev. Sci. Instrum.* **90**, 073901 (2019).
- ³¹<http://www.isis.stfc.ac.uk>, (Last accessed on January 2021).
- ³²L. A. Rodríguez Palomino, J. Dawidowski, J. I. Márquez Damián, G. J. Cuello, G. Romanelli, and M. Krzystyniak, “Neutron total cross-section of hydrogenous and deuterated 1- and 2-propanol and n-butanol measured using the vesuvio spectrometer,” *Nucl. Instrum. Methods Phys. Res. A* **870**, 84–89 (2017).
- ³³S. C. Capelli and G. Romanelli, “An effective hydrogen scattering cross section for time-of-flight neutron experiments with simple organic molecules,” *J. Appl. Crystallogr.* **52**, 1233–1237 (2019).
- ³⁴C. Andreani, R. Senesi, M. Krzystyniak, G. Romanelli, and F. Fernandez-Alonso, “Experimental studies of nuclear quantum effects in condensed matter: The case of water,” *Riv. del Nuovo Cim.* **41**, 291–340 (2018).
- ³⁵Marquez Damian, Jose Ignacio, Dawidowski, Javier, Granada, Rolando Jose, Cantargi, Florencia, Romanelli, Giovanni, Helman, Christian, Krzystyniak, Matthew, Skoro, Goran, and Roubtsov, Danila, “Experimental validation of the temperature behavior of the endf/b-viii.0 thermal scattering kernel for light water,” *EPJ Web Conf.* **239**, 14001 (2020).
- ³⁶G. Romanelli, S. Rudić, M. Zanetti, C. Andreani, F. Fernandez-Alonso, G. Gorini, M. Krzystyniak, and G. Škoro, “Measurement of the parahydrogen concentration in the isis moderators using neutron transmission and thermal conductivity,” *Nucl. Instrum. Methods Phys. Res. A* **888**, 88–95 (2018).
- ³⁷Cantargi, Florencia, Dawidowski, Javier, Helman, Christian, Márquez Damian, José Ignacio, Granada, Rolando Jose, Romanelli, Giovanni, Cuello, Julio Gabriel, Skoro, Goran, and Krzystyniak, Matthew, “Validated scattering kernels for triphenylmethane at cryogenic temperatures,” *EPJ Web Conf.* **239**, 14002 (2020).
- ³⁸Škoro, Goran, Romanelli, Giovanni, Rudić, Svemir, Lilley, Steven, and Fernandez-Alonso, Felix, “Discovery of new neutron-moderating materials at isis neutron and muon source,” *EPJ Web Conf.* **239**, 17008 (2020).
- ³⁹L. Rodríguez Palomino, J. Dawidowski, C. Helman, J. Márquez Damián, G. Romanelli, M. Krzystyniak, S. Rudić, and G. Cuello, “Determination of the scattering cross section of calcium using the vesuvio spectrometer,” *Nucl. Instrum. Methods Phys. Res., Sect. A* **927**, 443–450 (2019).
- ⁴⁰G. Romanelli, T. Minniti, G. Škoro, M. Krzystyniak, J. Taylor, D. Fornalski, and F. Fernandez-Alonso, “Visualization of the catalyzed nuclear-spin conversion of molecular hydrogen using energy-selective neutron imaging,” *J. Phys. Chem. C* **123**, 11745–11751 (2019).

- ⁴¹R. Ramos, F. Cantargi, J. I. M. Damian, and M. S. Goncalves-Carralves, "Study of thermal scattering for organic tissues through molecular dynamics," in *EPJ Web of Conferences*, Vol. 146 (EDP Sciences, 2017) p. 13008.
- ⁴²R. Ramos, M. S. Gonçalves-Carralves, and F. Cantargi, "Bioneutronics: Thermal scattering in organics tissues and its impact on bncr dosimetry," *Appl. Radiat. Isot.* **104**, 55–59 (2015).
- ⁴³K. S. Ytre-Hauge, K. Skjerdal, J. Mattingly, and I. Meric, "A monte carlo feasibility study for neutron based real-time range verification in proton therapy," *Sci. Rep.* **9**, 1–9 (2019).
- ⁴⁴C. Lee, S. Lee, S.-J. Lee, H. Song, D.-H. Kim, S. Cho, K. Jo, Y. Han, Y. H. Chung, and J. S. Kim, "Monte carlo simulation of secondary neutron dose for scanning proton therapy using fluka," *Plos one* **12**, e0186544 (2017).
- ⁴⁵J. N. Adkins, S. M. Varnum, K. J. Auberry, R. J. Moore, N. H. Angell, R. D. Smith, D. L. Springer, and J. G. Pounds, "Toward a human blood serum proteome: analysis by multidimensional separation coupled with mass spectrometry," *Molecular & Cellular Proteomics* **1**, 947–955 (2002).
- ⁴⁶L. M. Smith and N. L. Kelleher, "Proteoform: a single term describing protein complexity," *Nature methods* **10**, 186–187 (2013).
- ⁴⁷<http://www.sigmaaldrich.com>, (Last accessed on January 2021).
- ⁴⁸S. Cancelli, A. Muraro, E. P. Cippo, G. Romanelli, A. Abba, G. Grosso, G. Gorini, Z. Hu, C. Lai, O. M. Cormack, M. Tardocchi, S. Zhijia, J. Zhou, X. Zhou, and G. Croci, "Development of a ceramic double thick gem detector for transmission measurements at the vesuvio instrument at isis," *J. Inst (Under Submission)* (2021).
- ⁴⁹J. Binns, S. Parsons, and G. J. McIntyre, "Accurate hydrogen parameters for the amino acid l-leucine," *Acta Crystallogr., Sec. B* **72**, 885–892 (2016).
- ⁵⁰C. H. Görbitz and B. Dalhus, "L-isoleucine, redetermination at 120k," *Acta Crystallogr., Sec. C* **52**, 1464–1466 (1996).
- ⁵¹B. Dalhus, C. H. Görbitz, P. Kofod, *et al.*, "Crystal structures of hydrophobic amino acids i. redeterminations of l-methionine and l-valine at 120 k," *Acta Chemica Scandinavica* **50**, 544–548 (1996).
- ⁵²C. H. Görbitz, P. Karen, M. Dušek, and V. Petříček, "An exceptional series of phase transitions in hydrophobic amino acids with linear side chains," *IUCrJ* **3**, 341–353 (2016).
- ⁵³P. A. Williams, C. E. Hughes, and K. D. Harris, "L-lysine: Exploiting powder x-ray diffraction to complete the set of crystal structures of the 20 directly encoded proteinogenic amino acids," *Angewandte Chemie International Edition* **54**, 3973–3977 (2015).
- ⁵⁴J. Janczak, D. Zobel, and P. Luger, "L-threonine at 12 k," *Acta Crystallogr., Sec. C* **53**, 1901–1904 (1997).
- ⁵⁵C. C. Wilson, D. Myles, M. Ghosh, L. N. Johnson, and W. Wang, "Neutron diffraction investigations of l-and d-alanine at different temperatures: the search for structural evidence for parity violation," *New J. Chem.* **29**, 1318–1322 (2005).
- ⁵⁶C. Görbitz and B. Dalhus, "l-cysteine, monoclinic form, redetermination at 120k," *Acta Crystallogr., Sec. C* **52**, 1756–1759 (1996).
- ⁵⁷V. E. Bolyreva, N. E. Kolesnik, N. T. Drebuschak, H. Ahsbahs, and H.-P. Weber, "A comparative study of the anisotropy of lattice strain induced in the crystals of l-serine by cooling down to 100 k by increasing pressure up to 4.4 gpa," *Z. fur Kristallogr* **220** (2005).
- ⁵⁸J. J. Koenig, J.-M. Neudörfl, A. Hansen, and M. Breugst, "Redetermination of the solvent-free crystal structure of l-proline," *Acta Crystallogr., Sec. E* **74**, 1067–1070 (2018).
- ⁵⁹T. N. Drebuschak, E. V. Boldyreva, and E. S. Shutova, "β-glycine," *Acta Crystallogr., Sec. E* **58**, o634–o636 (2002).
- ⁶⁰E. Courvoisier, P. A. Williams, G. K. Lim, C. E. Hughes, and K. D. Harris, "The crystal structure of l-arginine," *Chemical Communications* **48**, 2761–2763 (2012).
- ⁶¹M. T. Ruggiero, J. Sibik, J. A. Zeitler, and T. M. Korter, "Examination of l-glutamic acid polymorphs by solid-state density functional theory and terahertz spectroscopy," *J. Phys. Chem. A* **120**, 7490–7495 (2016).
- ⁶²H. M. Cuppen, M. M. Smets, A. M. Krieger, J. A. van den Ende, H. Meeke, E. R. van Eck, and C. H. Görbitz, "The rich solid-state phase behavior of l-phenylalanine: Disappearing polymorphs and high temperature forms," *Crystal Growth & Design* **19**, 1709–1719 (2019).
- ⁶³A. Wagner and P. Luger, "Charge density and topological analysis of l-glutamine," *Journal of Molecular Structure* **595**, 39–46 (2001).
- ⁶⁴M. N. Frey, T. F. Koetzle, M. S. Lehmann, and W. C. Hamilton, "Precision neutron diffraction structure determination of protein and nucleic acid components. x. a comparison between the crystal and molecular structures of l-tyrosine and l-tyrosine hydrochloride," *J. Chem. Phys.* **58**, 2547–2556 (1973).
- ⁶⁵E.-e. Bendeif and C. Jelsch, "The experimental library multipolar atom model refinement of l-aspartic acid," *Acta Crystallogr., Sec. C* **63**, o361–o364 (2007).
- ⁶⁶K. Yamada, D. Hashizume, T. Shimizu, and S. Yokoyama, "l-asparagine," *Acta Crystallogr., Sec. E* **63**, o3802–o3803 (2007).
- ⁶⁷C. H. Görbitz, K. W. Törnroos, and G. M. Day, "Single-crystal investigation of l-tryptophan with z' = 16," *Acta Crystallogr., Sec. B* **68**, 549–557 (2012).
- ⁶⁸J. Madden, E. McGandy, N. Seeman, M. Harding, and A. Hoy, "The crystal structure of the monoclinic form of l-histidine," *Acta Crystallogr., Sec. B* **28**, 2382–2389 (1972).
- ⁶⁹A. Sjolander, "Multi-phonon processes in slow neutron scattering by crystals," *Arkiv Fysik* **14**, 315–371 (1958).
- ⁷⁰D. Parks, *Slow Neutron Scattering and Thermalization, with Reactor Applications* (W. A. Benjamin, 1970).
- ⁷¹X.-X. Cai and E. Klinkby, "Neutron total cross section calculation within the framework of quasi-harmonic approximation," *New J. Phys.* **19**, 103027 (2017).
- ⁷²G. L. Squires, "Introduction to the theory of thermal neutron scattering," **32**, 69 (1979).
- ⁷³J. Mayers, C. Andreani, and G. Baciocco, "Initial state effects in deep inelastic neutron scattering," *Phys. Rev. B* **39**, 2022–2028 (1989).
- ⁷⁴Y. Finkelstein and R. Moreh, "Temperature dependence of the proton kinetic energy in water between 5 and 673 K," *Chem. Phys.* **431**, 58–63 (2014).
- ⁷⁵G. Romanelli, B. Hewer, M. Krzystyniak, M. Gigg, R. Tolchenov, S. Mukhopadhyay, and F. Fernandez-Alonso, "Data analysis of neutron compton scattering experiments using MANTID," *J. Phys. Conf. Ser.* **1055**, 012016 (2018).
- ⁷⁶C. Andreani, C. Corsaro, D. Mallamace, G. Romanelli, R. Senesi, and F. Mallamace, "The onset of the tetrahobed structure in liquid water," *Sci. China Phys. Mech. Astron.* **62**, 107008 (2019).
- ⁷⁷C. Andreani, G. Romanelli, A. Parmentier, R. Senesi, A. I. Kolesnikov, H.-Y. Ko, M. F. Calegari Andrade, and R. Car, "Hydrogen dynamics in supercritical water probed by neutron scattering and computer simulations," *J. Phys. Chem. Lett.* **11**, 9461–9467 (2020).
- ⁷⁸G. Romanelli, M. Ceriotti, D. E. Manolopoulos, C. Pantalei, R. Senesi, and C. Andreani, "Direct measurement of competing quantum effects on the kinetic energy of heavy water upon melting," *The Journal of Physical Chemistry Letters* **4**, 3251–3256 (2013).
- ⁷⁹G. F. Syrykh, A. A. Stolyarov, M. Krzystyniak, G. Romanelli, and R. A. Sadykov, "Temperature dependence of the kinetic energy in the zr40be60 amorphous alloy," *JETP Letters* **105**, 591–594 (2017).
- ⁸⁰A. Perrichon, E. Jedvik Granhed, G. Romanelli, A. Piovano, A. Lindman, P. Hyldgaard, G. Wahnstrom, and M. Karlsson, "Unraveling the ground-state structure of bazo3 by neutron scattering experiments and first-principles calculations," *Chem. Mater.* **32**, 2824–2835 (2020).
- ⁸¹Y. Finkelstein, D. Nemirovsky, and R. Moreh, "Kinetic energy of oxygen atoms in water and in silica hydrogel," *Chem. Phys.* **533**, 110716 (2020).
- ⁸²P. Giannozzi, S. Baroni, N. Bonini, M. Calandra, R. Car, C. Cavazzoni, D. Ceresoli, G. L. Chiarotti, M. Cococcioni, I. Dabo, *et al.*, "Quantum espresso: a modular and open-source software project for quantum simulations of materials," *J. Condens. Matter Phys.* **21**, 395502 (2009).
- ⁸³D. Hamann, "Optimized norm-conserving vanderbilt pseudopotentials," *Phys. Rev. B* **88**, 085117 (2013).
- ⁸⁴A. Togo and I. Tanaka, "First principles phonon calculations in materials science," *Scripta Materialia* **108**, 1–5 (2015).
- ⁸⁵P. Ulpiani, G. Romanelli, D. Onorati, M. Krzystyniak, C. Andreani, and R. Senesi, "The effective isotropy of the hydrogen local potential in biphenyl and other hydrocarbons," *J. Chem. Phys.* **153**, 234306 (2020).
- ⁸⁶D. Onorati, C. Andreani, L. Arcidiacono, F. Fernandez-Alonso, G. Festa, M. Krzystyniak, G. Romanelli, P. Ulpiani, and R. Senesi, "Gamma background characterization on VESUVIO: before and after the moderator upgrade," *J. Phys. Conf. Ser.* **1055**, 012009 (2018).
- ⁸⁷D. Onorati, G. Romanelli, P. Ulpiani, C. Cazzaniga, E. Preziosi, L. Arcidiacono, G. Festa, C. Andreani, R. Senesi, and M. C. Morone, "Fluka simulations and benchmark measurements of the yap(ce) scintillators installed on the vesuvio spectrometer," *Nucl. Instrum. Methods Phys. Res. A*

- 969**, 164012 (2020).
- ⁸⁸P. Ulpiani, G. Romanelli, L. Arcidiacono, D. Onorati, G. Festa, M. Krzysztyniak, E. Schooneveld, F. Fernandez-Alonso, C. Andreani, and R. Senesi, "Enhancement of counting statistics and noise reduction in the forward-scattering detectors on the vesuvio spectrometer," *J. Phys. Conf. Ser.* **1055**, 012008 (2018).
- ⁸⁹D. L. Voi, F. d. O. Ferreira, R. C. Nunes, L. Carvalheira, and H. F. d. Rocha, "Analytical methods for analysis of neutron cross sections of amino acids and proteins," International Nuclear Atlantic Conference - INAC (2017).
⁹⁰<http://download.mantidproject.org>, (Last accessed on January 2021).
- ⁹¹C. Scatigno, G. Romanelli, E. Preziosi, M. Zanetti, S. F. Parker, S. Rudić, C. Andreani, and R. Senesi, "A python algorithm to analyze inelastic neutron scattering spectra based on the y-scale formalism," *J. Chem. Theory Comput.* **16**, 7671–7680 (2020).
- ⁹²S. F. Parker and P. I. Haris, "Inelastic neutron scattering spectroscopy of amino acids," *Spectroscopy* **22**, 297–307 (2008).
- ⁹³K. Ramić, C. Wendorff, Y. Cheng, A. I. Kolesnikov, D. L. Abernathy, L. Daemen, G. Arbanas, L. Leal, Y. Danon, and L. E. Liu, "Toward a better thermal scattering law of (c5o2h8)n: Inelastic neutron scattering and oclimax+njoy2016," *Ann. Nucl. Energy* **133**, 425 – 430 (2019).
- ⁹⁴S. Clark, M. Segall, C. Pickard, P. Hasnip, M. Probert, K. Refson, and M. Payne, "First principles methods using castep," *Zeitschrift für Kristallographie* **220**, 567–570 (2005).
- ⁹⁵K. Ramić, C. Wendorff, Y. Cheng, A. I. Kolesnikov, D. L. Abernathy, L. Daemen, G. Arbanas, L. Leal, Y. Danon, and L. E. Liu, "Thermal scattering law of c2h4n: Integrating experimental data with dft calculations," *Ann. Nucl. Energy* **120**, 778–787 (2018).
- ⁹⁶G. Sibona, R. Mayer, V. Gillette, C. Bonetto, and J. Granada, "Thermal neutron cross sections and diffusion parameters of plexiglass," *Ann. Nucl. Energy* **18**, 689–696 (1991).
- ⁹⁷D. A. Brown, M. Chadwick, R. Capote, A. Kahler, A. Trkov, M. Herman, A. Sonzogni, Y. Danon, A. Carlson, M. Dunn, *et al.*, "Endf/b-viii. 0: The 8th major release of the nuclear reaction data library with cielo-project cross sections, new standards and thermal scattering data," *Nuclear Data Sheets* **148**, 1–142 (2018).